Search for high entropy alloys in the X-NbTaTiZr systems (X = Al, Cr, V, Sn)

Search for high entropy alloys in the X-NbTaTiZr systems (X=Al,Cr,V,Sn)

M. G. Poletti[1*], G. Fiore[1], B.A. Szost[2], L. Battezzati[1]

[1]Dipartimento di Chimica, Università di Torino, Via P. Giuria 7, 10125 Torino, Italy

[2]Strategic & Emerging Technologies Team (TEC-TS), European Space Agency, ESTEC, 1 Keplerlaan, 2201 AZ Noordwijk, Netherlands

*corresponding author: marcogabriele.poletti@unito.it; tel. +390116707573

Abstract

High entropy alloys, i. e. solid solution phases are sought in the X-NbTaTiZr equiatomic system where the X element was chosen as Al, Cr, V and Sn by applying recent criteria based on size and electronegativity mismatch of alloy components, number of itinerant and total valence electrons, and the temperature at which the free energy of mixing changes at the alloy composition. The alloys containing V and Al are mostly constituted by solid solutions in good agreement with prediction.

Keywords: A. high-entropy alloys; B. casting; C. microstructure; D. X-ray diffraction.

1. Introduction

High entropy alloys (HEA) are solid solutions of simple crystal structure that contain usually five or more elements in equimolar amount. There is no predominant element in the system, therefore, solvent and solutes cannot be distinguished. A comprehensive review on these materials and general considerations on their metallurgy including the suggestion for precipitation hardening appeared recently in the literature [1, 2]. Due to their multicomponent constitution, there is a large number of potential HEA systems therefore extensive effort is required to predict the formation of solid solutions [3, 4]. Recently [5], we identified a series of parameters, based on Hume-Rothery Rules (HRR) and on a regular solution model description of the system, which proved useful in sorting out the multicomponent alloys known to date according to the occurrence of either solid solutions or other phases. The parameters refer to the atomic radius, r [6], and Allen electronegativity, χ, mismatch between the components [7, 8], denominated respectively δ and $\Delta\chi_{Allen}$:

$$\delta(\%) = 100 \cdot \sqrt{\sum_{i=1}^{n} c_i \cdot \left(1 - \frac{r_i}{r_a}\right)^2} \qquad (1)$$

$$\Delta\chi_{Allen}(\%) = 100 \cdot \sqrt{\sum_{i=1}^{n} c_i \cdot \left(1 - \frac{\chi_i}{\chi_a}\right)^2} \qquad (2)$$

where r_a and χ_a are the average radius and Allen electronegativity, respectively, and c_i is the concentration of the *i*-th element. The Allen scale is the most recent, physically based expression of electronegativity as the average ionization energy of the valence electrons (both theoretically and spectroscopically determined) for free atoms in their ground state [7, 8]. For the HEA compositions available in literature a map of δ versus $\Delta\chi_{Allen}$ shows a region corresponding to low values of both quantities where the occurrence of solid solutions, either a single one or coexisting *bcc* and *fcc*, is predominantly found (Fig. 1a).

The occurrence of *bcc*, *fcc* phases and intermetallic compounds in HEAs systems is also related to the number of itinerant *s* and *p* electrons, *e/a*, and the total valence electrons [9], *VEC*, of the alloy (Fig. 1b), as suggested by HRR: at higher values of VEC and lower values of *e/a* a *fcc* solid solution becomes stable; vice versa *bcc* solid solutions are experimentally found at low value of VEC and

higher value of e/a. Note that the region of *bcc* structures is discontinuous at VEC in transiting from 5 to 6 because the elements have 2 itinerant electrons (V) and 1 (Cr), respectively. The occurrence of compounds is related to the lower values of *e/a* per a fixed number of VEC.

A new parameter, μ, was also defined as

$$\mu = T_m/T_{SC} \qquad (3)$$

where T_m is the average melting temperature of the alloy [4]:

$$T_m = (\Sigma\ \Delta H_i^f\ c_i)/(\ \Sigma\ \Delta S_i^f\ c_i\ ) \qquad (4)$$

with ΔS_i^f, ΔH_i^f, and c_i: the entropy and enthalpy of fusion and concentration of i-th element, respectively, and T_{SC} is the temperature at which the hyper-surface describing the free energy of mixing changes curvature at spinodal points. The free energy of mixing was modelled according to the regular solution model with an interaction parameter expressed via the Miedema model [10].

The plot of μ versus δ reveals a tendency for the HEAs to occur at high values of μ, i. e. T_{SC} well below the melting point and, as in the previous plot, low values of radius mismatch (Fig. **1c**).

We elaborate on the previous work by Senkov [11] *et al.* who synthesised a new refractory HEA, HfNbTaTiZr, finding a single *bcc* solid solution with high room temperature ductility and yield

strength by exploring the replacement of a heavy metal, Hf, with a lighter one, resistant to oxidation at high temperature to which Ta and Nb refractory alloys are usually prone [12]. We recall that in all binary phase diagrams related to the quinary HfNbTaTiZr systems, no intermetallic compound is formed [13] whereas substituting a new element for Hf could likely induce the formation of intermetallic compounds instead of the desired solid solution. Intermetallic compounds albeit in limited quantity, may not be detrimental altogether since they could be exploited to harden the alloy by precipitation once an appropriate heat treatment is devised [2]. The elements selected to replace Hf are Al, V, Cr and Sn (Tab. 1). The addition of Al and V is expected to promote solid solutions being the parameters δ, $\Delta\chi_{Allen}$ and μ for these alloys (Tab. 2) located in regions of the map in Figs. 1 a-c where solid solutions have been found in other alloys; while the set of parameters for Cr and Sn indicate the likely occurrence of compounds.

2. Material and Methods

XNbTaTiZr ingots of about 20 g with X=Al,Cr,V,Sn were synthesized by arc melting in Ti gettered Ar atmosphere. Rods, sheets or lumps of the elements with purity better than 99.5 % were weighted to obtain equimolar composition; Every ingot was turned over and melted from 7 to 10 times to ensure homogeneous composition which was confirmed by EDS analysis at several points, including sections, as reported in Tab. 3. The ingots present shiny surfaces. All the samples have been cut, grinded, and polished in their cross section to obtain smooth surfaces for X-ray diffraction (XRD) (Cu-Kα radiation), Scanning Electron Microscopy (SEM) and energy-dispersive X-ray spectroscopy (EDS). Vickers Hardness was measured on the polished cross section using a 136° Vickers diamond pyramid under a 200 g load for 15 s; for each samples at least seven indentation have been measured.

3. Results

Backscattered electron images of the polished samples are reported in Figs. 2a and 2b for AlNbTaTiZr and in Figs. 2c and 2d for VNbTaTiZr. In both ingots the formation of composite microstructure constituted of dendrites and inter-dendritic regions is seen. According to EDS analysis (Tab. 4) the bright dendrites are rich in Ta (about 30 at %) while the inter-dendritic dark zones are rich in Zr (30 at %) in both cases. The concentration of Nb is slightly higher in the Ta-rich dendrite with respect to the black inter-dendritic zones. In the AlNbTaTiZr sample the Zr rich zones

are also richer in Al (about 25 at %). Ti is equally distributed between dendrites and inter-dendritic phases in both alloys. In VNbTaTiZr the V is equally distributed between the two main phases. Fig. 2b and 2d show backscattered electron images at higher magnification of the inter-dendritic dark zone for samples with Al and V, respectively: in both cases further minority phases occur across the inter-dendritic zones. In AlNbTaTiZr this phase is richer in Al and Zr with respect to the surroundings (about 40 at % in Zr and 30 at % in Al, Tab. 4). In VNbTaTiZr the minority phase is needle-like and displays a Z contrast with respect to its immediate surroundings, therefore, it is likely richer in light elements, like Zr, Ti and V, in which the adjacent region is then depleted.

X-ray diffraction patterns of the as-cast AlNbTaTiZr, VNbTaTiZr, CrNbTaTiZr, and SnNbTaTiZr alloys are shown in Figs. 3a to 3d. The number and position of reflections in Figs. 3a and 3b suggest the occurrence of *bcc* structures in as-cast alloys with Al and V. The patterns have also some additional reflections of low intensity, both at low 2θ values and close to the (110) *bcc* reflections, probably due to the minority Zr rich intermetallic compounds seen in the SEM images of Figs. 2c and d. Closer inspection of all reflections in the patterns related to the *bcc* structure, shows that they consist of multiple contributions that are compatible with two *bcc* solid solutions having distinct lattice parameters. These findings explain then the type of the main phases seen in SEM. Moreover, the blurring in backscattered SEM images (Fig. 2c and 2d**)** across the dendrites and inter-dendritic zones is found to be due to a concentration gradient within the two phases, suggesting that the broadening of the peaks in the X-ray pattern is not only due to internal stress but also to concentration gradients. We have indicatively determined the average lattice constants of the two solutions using all reflections in the patterns: a_{Al1}=3.325 Å, and a_{Al2}= 3.311 Å for the alloy containing Al and a_{V1}=3.316 Å, and a_{v2}= 3.289 Å for the alloy containing V. They must be considered with caution only to the purpose of identifying the phases in the SEM images using the element concentrations in Table 2 and applying Vegard law. The bright phases correspond to those having lower lattice constant because of the high Ta and low Zr content.

The microstructure of the as-cast CrNbTaTiZr sample (Figs. 4a and 4b) presents at least 4 phases with approximate compositions given in Tab. 4: a bright Ta-rich phase, a dark high-Zr phase, a dark grey phase where Zr and Cr predominate and a light grey Cr-rich phase. The reflections in the X-ray pattern are assigned to a *bcc* solid solution, the Ta-rich bright phase with lattice parameter a_{Cr1} = 3.302 Å. Since *bcc* reflections are broad and appear to display shoulders, it can be envisaged that a second *bcc* solid solution may occur also in this alloy although it cannot be identified with certainty. Then a *hcp* solid solution, Zr and Ti rich (darker contrast phase) and a C15 cubic Laves phase (a_{Laves} = 7.214 Å), Cr_2Zr structure are recognized.

The SnNbTaTiZr microstructure (Fig. 4c and 4d) presents at least three phases with approximate composition given in Tab. 3: a bright Ta-rich phase, a minority dark Ti-rich phase and a grey Zr and Sn-rich phase. The X-ray pattern of SnNbTaTiZr (Fig. 3d) contains many reflections probably due to a Sn-Zr intermetallic compound, in between them reflections can be recognized of the Ta-rich *bcc* solid solution, with lattice parameter of about 3.30 Å.

The Vickers hardness values of the as-cast samples are all rather high: AlNbTaTiZr 590 ± 18 HVN, VNbTaTiZr 467 ± 16 HVN, CrNbTaTiZr 599 ± 30 HVN, and SnNbTaTiZr 550 ± 46 HVN. The larger scatter is for the Sn containing alloy which has a duplex like appearance with comparable amounts of solid solution and intermetallic compounds. The hardness compare well with literature values [11] and, upon replacing the Hf with Al, V, and Cr, the hardness increased of 100-200 units.

4. Discussion

The multicomponent systems studied in this work confirm that the formation of solid solutions is strongly related to the difference in the atomic radius of the elements in the alloy. According to the atomic parameters reported in Tab **1**, the quaternary NbTaTiZr system from which the alloys analyzed here are derived has low radius mismatch, δ= 3.96 %, moreover in all the related eight binary systems no intermetallic compound is formed. The addition of Al (r=143 pm) and V (r=135 pm) is not expected to modify this microstructure since the mismatch becomes respectively 4.02 % and 5.53 %. The alloying of the smaller Cr (r_{Cr}=128 pm) would bring the mismatch to 7.1 %, above the limit for the formation of a solid solution (Fig. 1). With Sn instead (r_{Sn}=162 pm), a lower mismatch of 4.70% is induced which would allow the formation of a solid solution. The other factor, the difference in electronegativity, is respectively equal to 7.43, 5.30, 12.77, and 8.39 for the Al, V, Sn and Cr containing alloys. With a threshold value of 6, VNbTaTiZr should form a solid solution, CrNbTaTiZr, SnNbTaTiZr and AlNbTaTiZr should vice versa form compounds although the latter case is located near the border between two regions where either solid solutions or intermetallic compounds are experimentally found in literature (Fig. 1c).

Considering now the μ vs. δ map (Fig. 1c): only SnNbTaTiZr has a value of μ below 1 indicating that the estimated spinodal point temperature is higher with respect to the melting temperature. The μ parameter is favourable to the formation of solutions in the solid state for the other alloys.

According to the VEC vs e/a plot (Fig. 1c) the AlNbTaTiZr and VNbTaTiZr alloys should form a *bcc* solid solution, whereas CrNbTaTiZr and SnNbTaTiZr alloys should form intermetallic compounds.

Considering the whole set of parameters, the VNbTaTiZr (4 out of 4 favourable indicators) should give solid solutions as experimentally found. For AlNbTaTiZr (3 out of 4) the occurrence of solid solution is likely. On the other hand, the Cr-containing alloy only has a high value of μ, however intermetallic compounds are actually more stable than a solid solution. The SnNbTaTiZr is predicted to be intermetallic forming composition because of the high difference in electronegativity and the low value of the μ parameter in spite of the low radius mismatch.

The as-cast microstructures deserve further comments. VNbTaTiZr is composed of two disordered *bcc* phases, one rich in Ta and the other one rich in Zr. The low miscibility of Ta and Zr is apparently a predominant factor during the solidification from the melt. The observed microstructure suggests that the Ta-rich dendrites start to solidify first rejecting the Zr into the liquid which than solidifies as *bcc* with the final occurrence of the needle phase, Ti- and Zr-rich, probably the *hcp* solid solution expected at equilibrium at low temperature for these elements. It is worth to underline that in the binary phase diagrams of V with Ti, Zr, Nb, Ta only one intermetallic compound is found (Ta_2V stable up to 1310 °C).

Also for AlNbTaTiZr the Ta-rich dendrites solidify first leaving the liquid richer in Zr and Al from which the other *bcc* solution is formed together with a minority phase, probably a Zr-Al intermetallic compound.

CrNbTaTiZr is predicted to form intermetallic compounds, principally because of the small atomic radius of Cr with respect the other elements: in fact, it was experimentally found that a Cr-rich *fcc* Laves phase is formed in this system. Senkov [14] also synthesized a $CrMo_{0.5}NbTa_{0.5}TiZr$ alloy which was then isostatic pressed at T=1450 °C and P=207 MN/m^2 for 3h and annealed at T=1000°C for 100 h finding a *fcc* Laves phase and two *bcc* solid solutions; in our case a *hcp* phase has been experimentally found. Finally, the Sn containing alloy is expected to form intermetallic compounds as experimentally found. It is apparent that the microstructures reported in Figs. 2 and 4 are not at equilibrium since they result from quenching the melt by the cooled Cu heart of the arc melter, Most of the phases are actually found in equilibrium in binary or ternary systems of the alloy components, however, it is expected that their volume fraction, grain shape and local composition might vary upon annealing. Further work is under way to elucidate this, however, the present microstructures should be relevant for various near net shape manufacturing processes which could be exploited for component forming.

The hardness is high for all alloys containing some amount of intermetallic phases, e. g. the phase mixture in the CrNbTaTiZr sample showed the higher hardness. It is notable that the alloy containing V which is mostly constituted of two *bcc* solutions, is substantially hard indicating that the internal stress of the solutions contributes to its strength.

5. Conclusions

The parameters developed in [5] have been applied to the X-NbTaTiZr systems, with X=Al, V, Cr and Sn, to predict the formation of either intermetallic compounds or solid solutions. They are based on the radius and electronegativity mismatch of elements, the number of valence and itinerant electrons in the alloy and the curvature of the free energy curve of the solid solution (μ parameter). The overall approach proved sound. In fact the alloys containing Al or V have parameter values in agreement with the formation of solid solution, while the alloys with Sn and Cr are predicted to form intermetallics. SEM and XRD analysis of cast alloys showed that VNbTaTiZr and AlNbTaTiZr are actually constituted by two bcc solid solutions, wheras in CrNbTaTiZr a bcc and a hcp solid solution plus a Laves intermetallic phase are present and in SnNbTaTiZr the bcc solid solution is not the majority phase since intermetallic compounds occur in large quantity.

Acknowledgments

This work has been performed in the frame of the EU-7FP Accelerated Metallurgy Project (ACCMET, contract NMP4-LA-2011-263206).

References

[1] Y. Zhang, T.T. Zuo, Z. Tang, M.C Gao., K.A Dahmen., P.K. Liaw, et al., Prog Mater Sci 61 (2014) 1.

[2] D.B. Miracle, J.D Miller, O.N. Senkov, C. Woodward, M.D Uchic, J. Tiley, Entropy 16 (2014) 494.

[3] X. Yang, Y. Zhang, Mater Chem Phys 132 (2012) 233.

[4] S. Guo, C.T. Liu, Prog Nat Sci Mater Int 21 (2011) 433.

[5] M.G. Poletti, L. Battezzati, Acta Materialia 75 (2014) 297.

[6] E. Teatum, K. Gschneidner, J. Waber, Compilation of calculated data useful in predicting metallurgical behaviour of the elements in binary alloy systems. Los Alamos Scientific Laboratory, LA-2345; 1960.

[7] J.B. Mann, T.L. Meek, C. Leland, L.C. Allen, J Am Chem Soc 122 (2000) 2780.

[8] J.B. Mann,T.L. Meek, E.T. Knight, J.F. Capitani, L.C. Allen, J Am Chem Soc 122 (2000)n5132.

[9] S. Guo, C. Ng,J. Lu, C.T. Liu, J Appl Phys 109 (2011) 103505.

[10] A. Takeuchi, A. Inoue, Mater Trans 46 (2005) 2817.

[11] O.N. Senkov, J.M. Scotta, S.V. Senkova, D.B. Miracle, C.F. Woodward, J Alloys Compd 509 (2011) 6043.

[12] B.A.Pint,J.R. DiStefano, I.G. Wright, Mater Sci Eng A 415 (2006) 260.

[13] H. Okamoto, Desk Handbook: Phase Diagrams for Binary Alloys. ASM International; 2000.

[14] O.N. Senkov,F. Zhang, J.D. Miller, Entropy 15 (2013) 3796

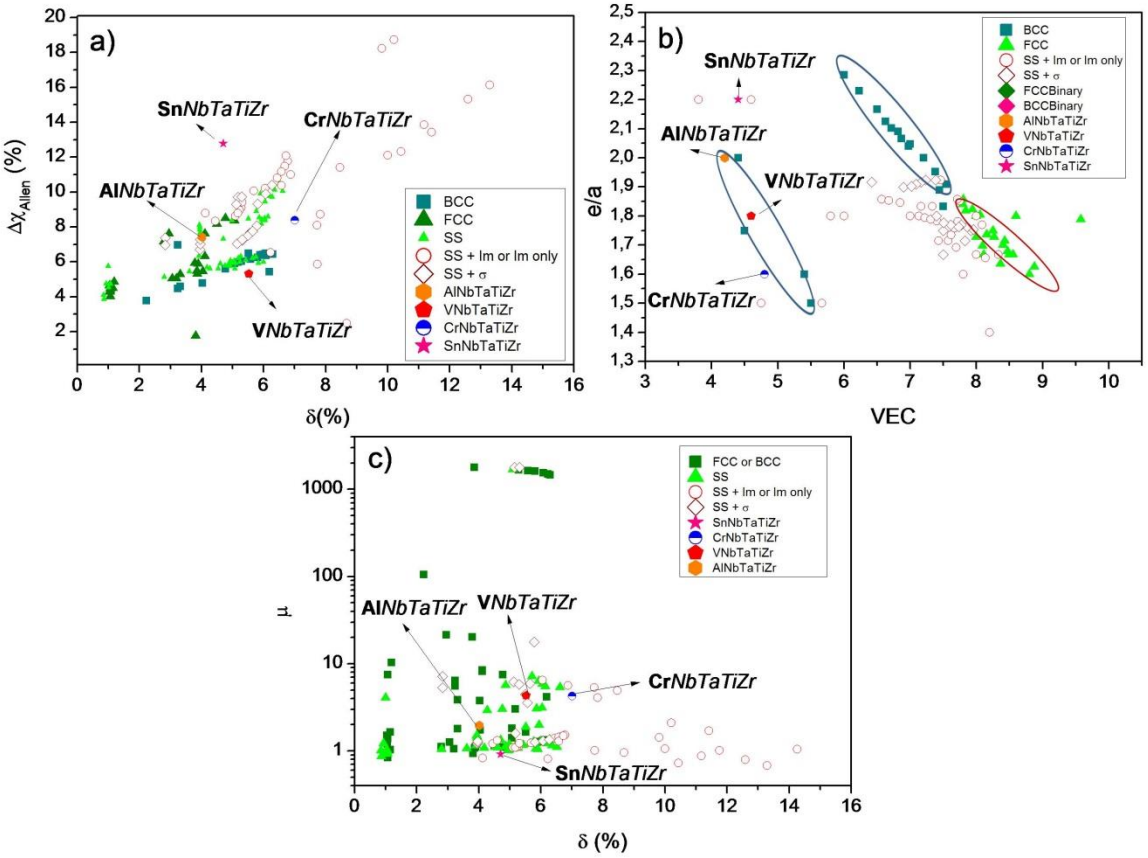

Figure 1. HEA maps from [5], (a) radius (Eq. 1) and Allen electronegativity mismatch (Eq. 2) for HEA systems from literature, (b) valence electron, VEC, and itinerant electrons per atom, e/a, for HEA systems from literature, (c) μ parameter (Eq. 3) versus radius mismatch (Eq. 1). BCC and FCC stands for formation of only one phase, SS stands for formation of more solid solutions, SS + IM for formation of solid solution and compounds or only compounds, SS + σ for systems where the formation of solid solution plus σ phase occurs.

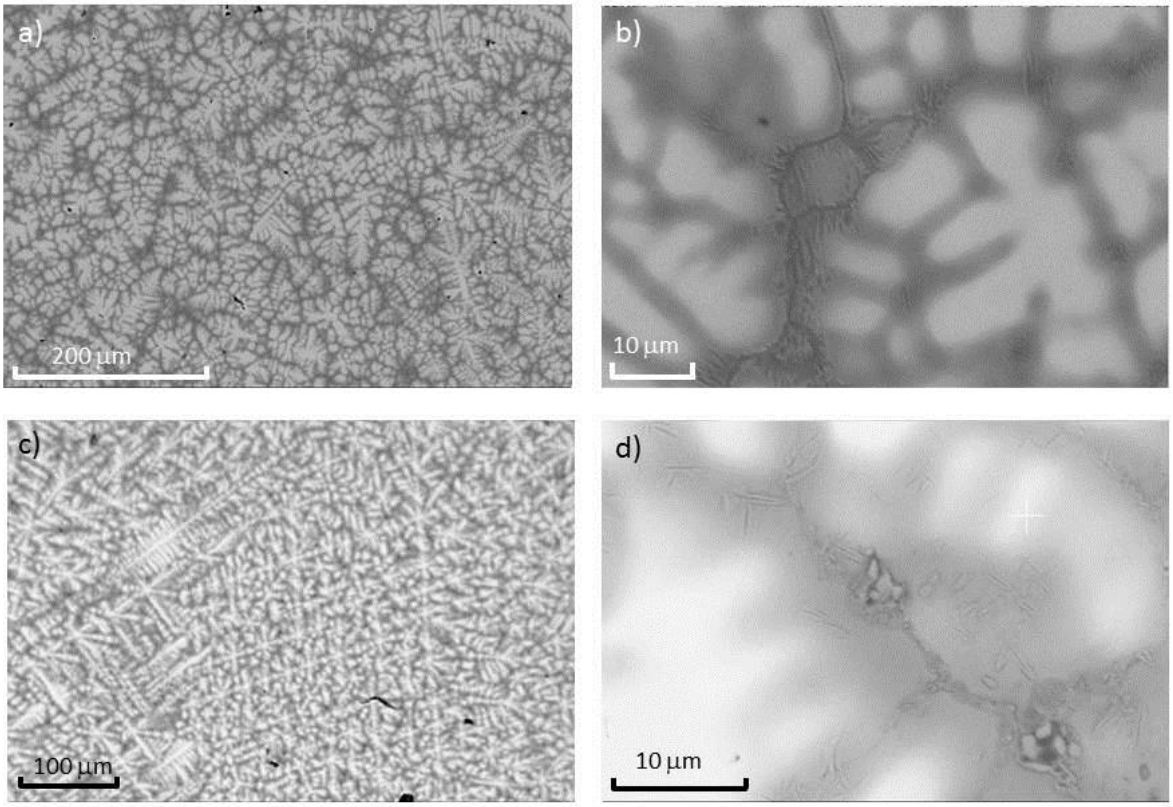

Figure 2. Backscattering electron microscope images of as-cast AlNbTaTiZr (a), VNbTaTiZr (c), and magnified images showing inter-dendritic phases in AlNbTaTiZr (b), and VNbTaTiZr (d).

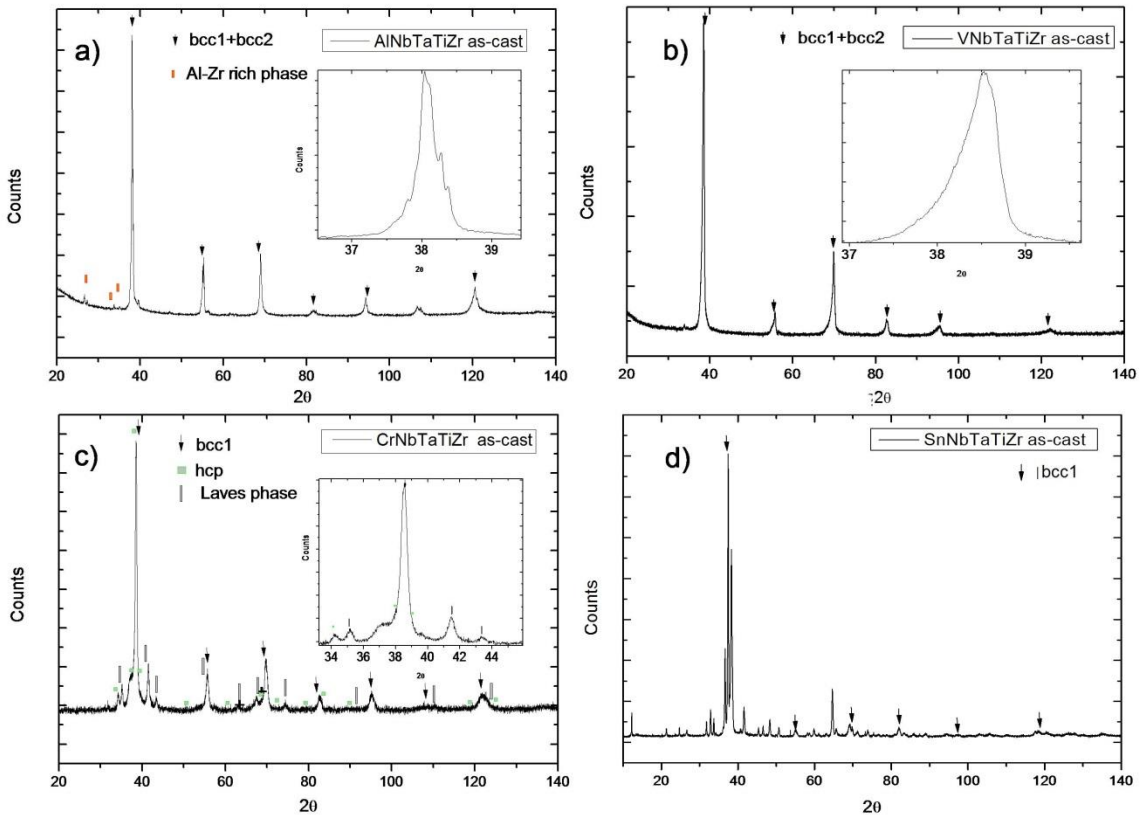

Figure 3. X-ray pattern of as-cast AlNbTaTiZr (inset shows the region of the (110) reflection) (a), VNbTaTiZr, (inset shows the region of the (110) reflection) (b), CrNbTaTiZ (inset shows the reflectionss between 34°<2θ< 44°) (c), and SnNbTaTiZr (d). The portion of pattern displayed in the inset of Fig. 3a is made of six contributions. The two small reflections seen as humps at higher angles are compatible with a Zr-Al compound. The two major overlapping reflections are precisely assigned to a *bcc* phase with partially resolved CuKα1 and CuKα2 contributions. Analogously the two minor reflections at higher angles are due to the second *bcc* solid solution. The composite reflections at higher angles can all be explained accordingly. The inset of Fig. 3b is indicative of overlapping (110) *bcc* reflections as for all the others in the whole pattern.

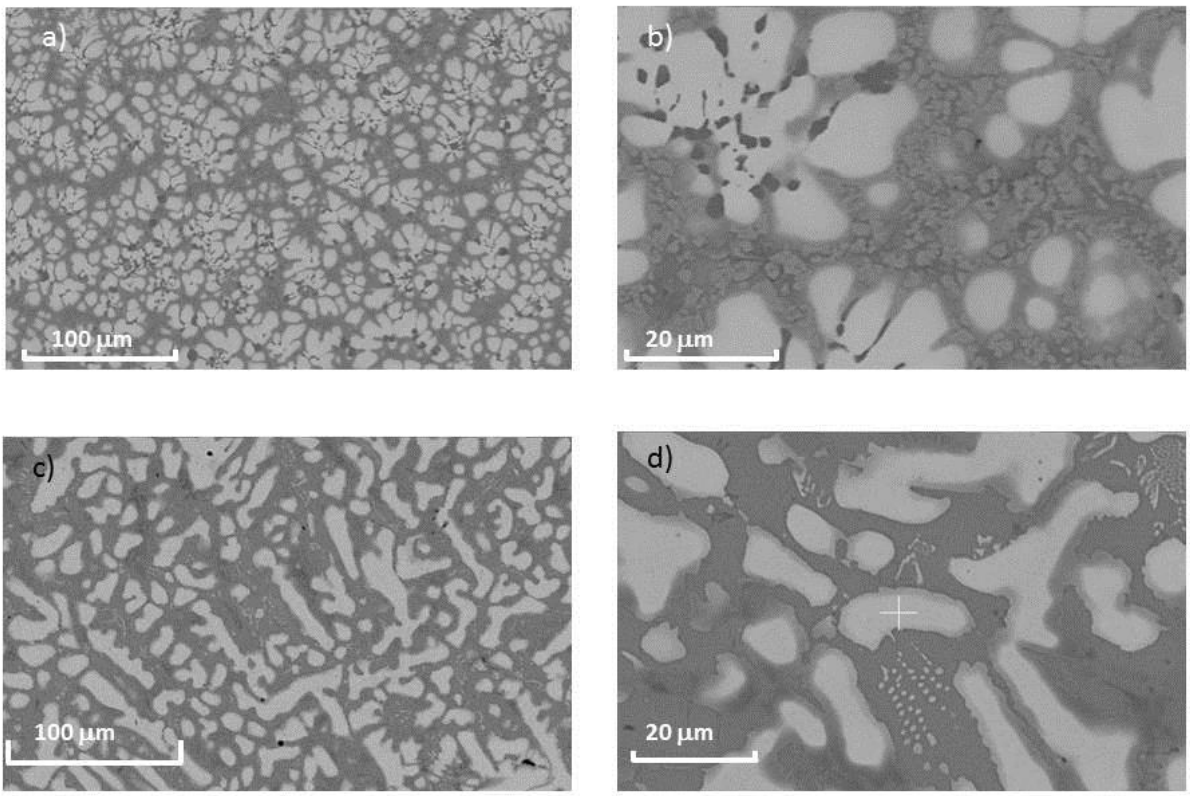

Figure 4. Backscattering electron microscope images of as-cast CrNbTaTiZr (a), SnNbTaTiZr (c), and magnified images of CrNbTaTiZr (b), and SnNbTaTiZr (d).

	Al	V	Cr	Sn	Nb	Ta	Ti	Zr
Atomic radius (pm)	143	135	128	162	147	147	146	160
Allen Electronegativity	1,61	1,53	1,65	1,82	1,41	1,34	1,38	1,32
VEC	3	5	6	4	5	5	4	4
e/a	3	2	1	4	1	2	2	2

Table 1. Atomic radius [6], Allen electronegativity [7,8], VEC and *e/a* values for the elements used in this work.

Alloy	δ	$\Delta\chi_A$	VEC	e/a	μ
AlNbTaTiZr	4,02	7,43	4,2	2	1,98
VNbTaTiZr	5,53	5,30	4,60	1,80	4,31
SnNbTaTiZr	4,70	12,77	4,40	2,20	0,89
CrNbTaTiZr	7,01	8,39	4,80	1,60	4,25

Table 2. Values of parameters obtained in [5] for X-NbTaTiZr where X=Al, V, Cr, and Sn for the HEA synthesized in this work.

Alloy	X	Nb	Ta	Ti	Zr
AlNbTaTiZr	(Al) 20	19	21	20	20
VNbTaTiZr	(V) 21	20	20	20	19
CrNbTaTiZr	(Cr) 17	20	21	19	23
SnNbTaTiZr	(Sn) 19	19	20	18	23

Table 3. Composition of as-cast HEAs samples determined by EDS analysis.

AlNbTaTiZr as-cast	Al	Nb	Ta	Ti	Zr
dark phase	25	14	10	20	31
bright phase	18	23	29	20	10
VNbTaTiZr as-cast	V	Nb	Ta	Ti	Zr
dark phase	20	16	10	21	33
bright phase	20	24	29	20	7
CrNbTaTiZr as-cast	Cr	Nb	Ta	Ti	Zr
bright phase	10	29	39	16	6
dark phase	2	5	5	18	70
Dark grey phase	24	13	9	20	34
light grey phase	42	12	15	12	19
grey phase	53	10	19	11	7
SnNbTaTiZr as cast	Sn	Nb	Ta	Ti	Zr
bright phase	8	30	44	14	4
dark phase	14	22	10	43	11
grey phase	37	5	2	13	43

Table 4 Composition of phases in the alloys synthesized in this work as determined by EDS analysis.